

Slow surface plasmon pulse excitation in metal-insulator-metal plasmonic waveguide with chirped grating

Joonsoo Kim,¹ Seung-Yeol Lee,¹ Hyeonsoo Park,¹ Hwi Kim,² and ByoungHo Lee^{1,*}

¹National Creative Research Center for Active Plasmonics Application Systems, Inter-University Semiconductor Research Center and School of Electrical Engineering, Seoul National University, Gwanak-Gu Gwanakro 1, Seoul 151-744, South Korea

²ICT Convergence Technology for Health & Safety and Department of Electronics and Information Engineering, Korea University, 2511 Sejong-ro, Sejong 339-700, South Korea
byoungho@snu.ac.kr

Abstract: A scheme for the excitation of slow surface plasmon pulses using photonic interband transition in a metal-insulator-metal (MIM) waveguide is proposed. An investigation the mode transition behavior inside the binary grating confirmed that the proposed concept can be understood in terms of the coupling of symmetric and anti-symmetric plasmonic modes. We observed that, although a binary grating that is optimized for a single frequency can excite slow surface plasmon pulses, it is inadequate for broadband mode conversion. To rectify this, a chirped grating was designed for the demonstration of broadband mode conversion by applying a cascade mode transition with different frequencies.

©2014 Optical Society of America

OCIS codes: (250.5403) Plasmonics; (230.7390) Waveguides, planar; (200.4490) Optical buffers; (320.5550) Pulses.

References and links

1. S. A. Maier, *Plasmonics: Fundamentals and Applications* (Springer, 2007).
2. H. Choo, M.-K. Kim, M. Staffaroni, T. Seok, J. Bokor, S. Cabrini, P. J. Schuck, M. C. Wu, and E. Yablonovich, "Nanofocusing in a metal-insulator-metal gap plasmon waveguide with a three-dimensional linear taper," *Nat. Photonics* **6**(12), 838–844 (2012).
3. K.-Y. Kim, J. Kim, I.-M. Lee, and B. Lee, "Analysis of transverse power flow via surface modes in metamaterial waveguides," *Phys. Rev. A* **85**(2), 023840 (2012).
4. J. Park, K.-Y. Kim, I.-M. Lee, H. Na, S.-Y. Lee, and B. Lee, "Trapping light in plasmonic waveguides," *Opt. Express* **18**(2), 598–623 (2010).
5. K. L. Tsakmakidis, A. D. Boardman, and O. Hess, "'Trapped rainbow' storage of light in metamaterials," *Nature* **450**(7168), 397–401 (2007).
6. M. S. Jang and H. Atwater, "Plasmonic rainbow trapping structures for light localization and spectrum splitting," *Phys. Rev. Lett.* **107**(20), 207401 (2011).
7. H. Hu, D. Ji, X. Zeng, K. Liu, and Q. Gan, "Rainbow trapping in hyperbolic metamaterial waveguide," *Sci. Rep.* **3**, 1249 (2013).
8. Q. Gan, Y. Gao, K. Wagner, D. Vezhenov, Y. J. Ding, and F. J. Bartoli, "Experimental verification of the rainbow trapping effect in adiabatic plasmonic gratings," *Proc. Natl. Acad. Sci. U.S.A.* **108**(13), 5169–5173 (2011).
9. L. V. Hau, S. E. Harris, Z. Dutton, and C. H. Behroozi, "Light speed reduction to 17 metres per second in an ultracold atomic gas," *Nature* **397**(6720), 594–598 (1999).
10. G. Heinze, C. Hubrich, and T. Halfmann, "Stopped light and image storage by electromagnetically induced transparency up to the regime of one minute," *Phys. Rev. Lett.* **111**(3), 033601 (2013).
11. T. Baba, "Slow light in photonic crystals," *Nat. Photonics* **2**(8), 465–473 (2008).
12. A. Yariv, "Couple-mode theory for guided-wave optics," *IEEE J. Quantum Electron.* **9**(9), 919–933 (1973).
13. H. A. Haus and W. Huang, "Coupled-mode theory," *Proc. IEEE* **79**(10), 1505–1518 (1991).
14. D. M. Beggs, I. H. Rey, T. Kampfrath, N. Rotenberg, L. Kuipers, and T. F. Krauss, "Ultrafast tunable optical delay line based on indirect photonic transitions," *Phys. Rev. Lett.* **108**(21), 213901 (2012).
15. M. Castellanos Muñoz, A. Y. Petrov, L. O'Faolain, J. Li, T. F. Krauss, and M. Eich, "Optically induced indirect photonic transitions in a slow light photonic crystal waveguide," *Phys. Rev. Lett.* **112**(5), 053904 (2014).
16. C. R. Otey, M. L. Povinelli, and S. Fan, "Completely capturing light pulses in a few dynamically tuned microcavities," *J. Lightwave Technol.* **26**(23), 3784–3793 (2008).
17. C. R. Otey, M. L. Povinelli, and S. Fan, "Capturing light pulses into a pair of coupled photonic crystal cavities," *Appl. Phys. Lett.* **94**(23), 231109 (2009).

18. H. Kim, J. Park, and B. Lee, *Fourier Modal Method and Its Applications in Computational Nanophotonics* (CRC Press, 2012).
 19. M. G. Blaber, M. D. Arnold, and M. J. Ford, "Search for the ideal plasmonic nanoshell: the effect of surface scattering and alternatives to gold and silver," *J. Phys. Chem. C* **113**(8), 3041–3045 (2009).
 20. Z. Yu and S. Fan, "Complete optical isolation created by indirect interband photonic transitions," *Nat. Photonics* **3**(2), 91–94 (2009).
 21. H. Kim and B. Lee, "Efficient frequency conversion in slab waveguide by cascaded nonreciprocal interband photonic transitions," *Opt. Lett.* **35**(19), 3165–3167 (2010).
 22. H. Lira, Z. Yu, S. Fan, and M. Lipson, "Electrically driven nonreciprocity induced by interband photonic transition on a silicon chip," *Phys. Rev. Lett.* **109**(3), 033901 (2012).
-

1. Introduction

Plasmonics enables the excitation and manipulation of strongly confined electromagnetic fields in the deep subwavelength region. High-intensity electric fields in plasmonic structures can enhance the interaction between light and matter and this can be usefully applied to the design of integrated optical devices and nonlinear optics. In particular, metal-insulator-metal (MIM) waveguides have been considered for use as effective structures for confining guided waves in the several tens of nanometers due to the surrounding metallic walls [1, 2]. More interestingly, in metallic walls of waveguides, the direction of the phase and energy flow can be opposite because of the negative permittivity of metals [3]. As a result of the negative power flow, it has been reported that sufficiently thin MIM waveguides can be utilized to support stopped wavepackets when the power flows in the dielectric core and metallic cladding are balanced [4]. The usual strategy for obtaining stopped wavepackets involves the use of tapered structures, so-called the 'rainbow trapping waveguides' [5–8]. It has been reported that tapered metamaterial waveguides or chirped gratings for spoof plasmons are capable of stopping light of different colors at different positions. However, less attention has been focused on the potential use of non-tapered waveguides, since slow wavepackets will not propagate from one end to the middle of a plasmonic waveguide. Here, we note that there are other slow light mechanisms, including electromagnetically induced transparency [9, 10] or Bragg reflections in photonic crystals [11]. However, to retain atomic coherence, electromagnetically induced transparency requires cryogenic conditions, and photonic crystal devices are generally much larger than plasmonic ones.

On the other hand, the induction of photonic interband transition using gratings or the time dependent modulation of permittivity is a well-known strategy in guided optics [12, 13]. The theoretical basis of this discipline is usually explained by the coupled mode theory in the case of weak perturbation, and oscillatory energy transfer between coupled modes is understood to be universal in such systems. Attempts have been made to realize efficient optical delay lines or optical buffers by using photonic interband transitions in photonic crystals [14, 15] or dynamically modulated coupled cavity systems [16, 17]. The use of a photonic interband transition can be useful for the excitation of slow light pulses inside a waveguide because designing an active device is much easier compared to tapered waveguides. However, dynamic photonic crystal-based devices not only generally have large footprints but also convert input pulses to slow light incompletely. The complete trapping of light has been achieved in [16], but a complicated temporal modulation of permittivity was required. Hence, the next step would be the design of a spatial permittivity profile that enables efficient conversion to slow light with simple on/off or harmonic temporal modulation.

In this paper, we report on an analysis of the mode transition behavior caused by gratings in MIM waveguides that supports both slow ($n_g \approx 83.1$) anti-symmetric plasmonic modes and relatively fast ($n_g \approx 22.6$) symmetric plasmonic modes. We first designed a binary grating that optimally couples the symmetric mode to the anti-symmetric mode at a single frequency. Pulse simulation showed that optimized gratings can excite slow plasmonic pulses, but the conversion is efficient only within a small spectral interval, leaving a portion of the incident pulse unconverted. In order to eliminate this unconverted residual pulse which originates from the resonant narrowband nature of the grating, we designed a chirped grating. The

findings show that this chirped grating enables the nearly complete conversion of incident pulses into slow plasmonic mode pulses. The Fourier modal method (FMM) which has advantages for modal analysis was used for the simulations throughout this work [18].

2. Proposed structure and design of MIM waveguide

A conceptual illustration of the proposed structure is depicted in Fig. 1(a). The guided modes considered for modal transitions are the symmetric and anti-symmetric plasmonic modes that exist in the MIM waveguide. In our case, a pulse of the symmetric plasmonic mode is the input excitation because it is faster and less propagation loss is involved, compared to the anti-symmetric mode. Inside an MIM waveguide, a grating that occupies half of the MIM core is introduced for waveguide mode conversion. When the incident pulse meets the grating, a photonic interband transition from the symmetric mode to the anti-symmetric mode occurs, provided the difference between the propagation constants of the two modes is correctly compensated by the grating momentum. Grating parameters such as the grating period, index difference, and grating length should be carefully designed for efficient mode transition. In this section, we focus on an analysis of the MIM waveguide mode dispersion relationship and estimation of the optimal grating period. Optimization of the waveguide grating is described in later sections. To model electromagnetic response of metal, we used the Drude model:

$$\epsilon_m(\omega) = 1 - \frac{\omega_p^2}{\omega^2 + i\gamma\omega}, \quad (1)$$

where it is assumed that the metal has the plasma frequency of gold ($\omega_p = 8.55$ eV) [19] and a negligible damping constant ($\gamma = 1.84$ μ eV). Note that we examine a nearly lossless case to separate exponential decay from mode transition behavior.

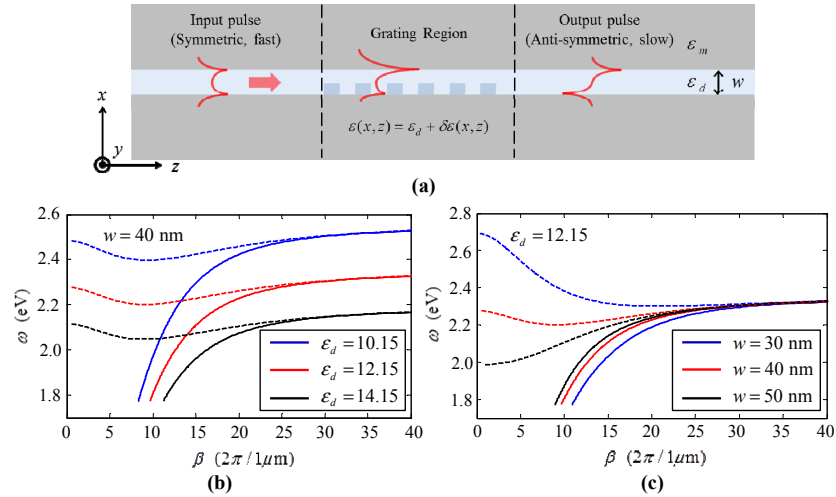


Fig. 1. (a) Schematic of the proposed structure. A grating inside an MIM waveguide ($w = 50$ nm, $\epsilon_d = 12.15$) couples symmetric and anti-symmetric modes. It converts symmetric mode pulse of temporal width 200 fs to 4-fold slower anti-symmetric pulse. Waveguide dispersion relation depending on (b) the permittivity of core material and (c) the width of waveguide. Solid and dashed lines represent symmetric and anti-symmetric plasmonic modes respectively.

Figures 1(b) and 1(c) show plots of the dispersion relation of the symmetric and anti-symmetric modes with varying waveguide width and permittivity of the dielectric region, in order to find an appropriate value for the slow anti-symmetric mode. It has been reported that the conditions for the existence of a stopped anti-symmetric mode in MIM waveguides is

given by $1 < -\text{Re}[\epsilon_m / \epsilon_d] < 1.28$ [4]. Therefore, the permittivity of the core dielectric material determines the frequency range of the stopped anti-symmetric modes, as shown in Fig. 1(b). For this work, we chose the dielectric to be Si ($\epsilon_d = 12.15$) which fixes our frequencies of interest at around 2.05eV, roughly corresponding to a free space wavelength of 600 nm.

From Fig. 1(c), we can observe how the width of the MIM waveguide affects the dispersion relation. According to the explanation in [4], the power flow through the metal region is in the opposite direction to the phase flow, whereas they are in the same direction within the dielectric region. When the width of the waveguide is changed, the portion of the field occupying the metal and dielectric regions is also changed. As the waveguide becomes thinner, the portion of power flow on the metal increases; hence, the anti-symmetric mode becomes a backward mode since the direction of group velocity is determined by the net flow of the metal and the dielectric region. On the other hand, when the waveguide becomes thick, the power transmission through the dielectric becomes large, and then the anti-symmetric mode becomes a forward mode. Between these two extremes, it is possible for forward and backward modes to exist simultaneously in MIM waveguides and the slow light dispersion appears near the mode degeneracy. In this study, we set the waveguide width at 50 nm in order to obtain a group velocity ratio for the two modes ($v_{g,\text{ant}} / v_{g,\text{sym}} \approx 0.27$). As depicted in Fig. 2, the selected central wavelength and spectral bandwidth of the input pulse are $\lambda_0 = 613$ nm and $\Delta\lambda = 10$ nm (corresponding to a temporal width of $\Delta t = 200$ fs), respectively. The repetition period is assumed to be $T = 10$ ps and 81 rounds of FMM simulations were needed to express the Gaussian pulse input.

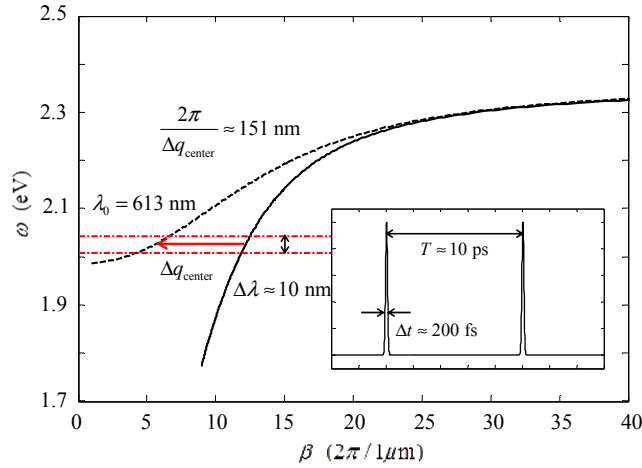


Fig. 2. Dispersion relation of the symmetric (black solid) and anti-symmetric (black dashed) modes for MIM waveguide ($w = 50$ nm, $\epsilon_d = 12.15$). Red dash-dotted lines mark the linewidth of the input pulse. The inset shows the shape of the input pulse in the temporal domain.

3. Design of a binary grating and its pulse response

As a first step, we consider a simple periodic binary grating. To design such a grating, we applied the coupled mode theory for waveguides which works well for small perturbations. Given the permittivity profile $\epsilon(x)$ and sinusoidal perturbation $\delta\epsilon(x, z) = \Delta\epsilon(x) \cos(qz)$, the governing equation of the waveguide is the Helmholtz equation:

$$\left[\nabla^2 + \epsilon(x) \frac{\omega^2}{c^2} \right] U = -\delta\epsilon(x, z) \frac{\omega^2}{c^2} U, \quad (2)$$

where $U(x, z, t)$ can be either a component of the electric or magnetic field. Considering two waveguide modes of interest with propagation constants β_1 and β_2 , we can express the electromagnetic field in the waveguide as a linear combination of two modes with coefficients that vary along the direction of propagation:

$$U(x, z, t) = a_1(z)U_1(x)e^{i(\beta_1 z - \omega t)} + a_2(z)U_2(x)e^{i(\beta_2 z - \omega t)}. \quad (3)$$

Substituting this expression into the Helmholtz Eq. (2) gives the differential equations for coefficients which are called the coupled mode equation:

$$\begin{aligned} \frac{da_1}{dz} &= i \frac{\kappa}{\beta_1} a_2 e^{-i\Delta z}, \\ \frac{da_2}{dz} &= i \frac{\kappa^*}{\beta_2} a_1 e^{i\Delta z}. \end{aligned} \quad (4)$$

Here, $\Delta = \beta_1 + q - \beta_2$ is called the detuning factor and κ is the coupling coefficient proportional to the overlap integral of the form $\int_{-\infty}^{\infty} U_1^*(x) \Delta \epsilon(x) U_2(x) dx$, which implies that the anti-symmetric part of the transverse permittivity profile is responsible for the coupling between the symmetric and anti-symmetric modes. Therefore, the grating is designed so as to asymmetrically fill half of the core as shown in Fig. 1(a). Solving this equation for the initial conditions, $a_1(0) = 1$, and $a_2(0) = 0$, gives the following expressions for the modal population [12]:

$$\begin{aligned} |a_1|^2 &= \frac{2|\kappa|^2 + \beta_1 \beta_2 \Delta^2}{4|\kappa|^2 + \beta_1 \beta_2 \Delta^2} + \frac{2|\kappa|^2}{4|\kappa|^2 + \beta_1 \beta_2 \Delta^2} \cos \left(\sqrt{\frac{4|\kappa|^2}{\beta_1 \beta_2} + \Delta^2} z \right), \\ |a_2|^2 &= \frac{\beta_2}{\beta_1} \left[\frac{2|\kappa|^2}{4|\kappa|^2 + \beta_1 \beta_2 \Delta^2} - \frac{2|\kappa|^2}{4|\kappa|^2 + \beta_1 \beta_2 \Delta^2} \cos \left(\sqrt{\frac{4|\kappa|^2}{\beta_1 \beta_2} + \Delta^2} z \right) \right]. \end{aligned} \quad (5)$$

From Eq. (5), it can be seen that complete energy transfer from mode 1 to 2 is possible only when the detuning factor is zero. This condition is called the phase matching condition or perfect momentum compensation and it is widely used in the design of grating periods. We note that arbitrary periodic gratings of the same period work similarly to cosine gratings except that higher order harmonic terms also need to be considered.

Now, we design a binary grating that completely converts the symmetric mode to the anti-symmetric mode of the MIM waveguide. The optimal grating period can be estimated from the phase matching condition. Where the optimal grating period varies with the frequency, we choose the central frequency of the input pulse as a representative frequency. The difference in permittivity between silicon and the perturbed dielectric is fixed at 0.4 and the fill factor is set at 0.5. We note that it is not necessary for the grating strength and fill factor to be fixed at these values for complete mode conversion. As will be clear in Fig. 3(b), for a different choice of grating strength, complete mode conversion can be done by a fine tuning of the grating period and appropriate adjustment of the grating length. An adjustment of the fill factor is essentially the same as a change in grating strength in the sense that both changes the coupling coefficient of the symmetric and anti-symmetric modes, but do not change the detuning factor. Hence, we can choose different set of grating strengths and fill factors in designing a mode converter.

The optimal grating period was found by a parametric study near the estimated value deduced from the dispersion relation in Fig. 2. Figure 3(a) shows the oscillatory modal energy transfer inside the binary grating when the symmetric mode is launched from the left side of

the grating. Since we should design the grating to have the largest conversion efficiency with shortest possible grating length, we marked the optimal number of periods as N_{opt} , where the modal population of the symmetric mode is the smallest, as indicated in Fig. 3(a). For each grating period Λ , we adjusted the grating length at $N_{\text{opt}}(\Lambda)$ and obtained the normalized output power flow for the anti-symmetric mode, as shown in Fig. 3(b). The result showed that complete mode conversions were possible for grating strengths 0.2, 0.3 and 0.4. The optimal grating period shifts from the estimated value ($\Lambda = 151$ nm) with increasing grating strength. The optimal grating length was $\Lambda \approx 159$ nm for $\Delta\epsilon = 0.4$. The difference in the optimal grating period from the estimated value is due to the change in modal index caused by the symmetric part of the permittivity perturbation profile.

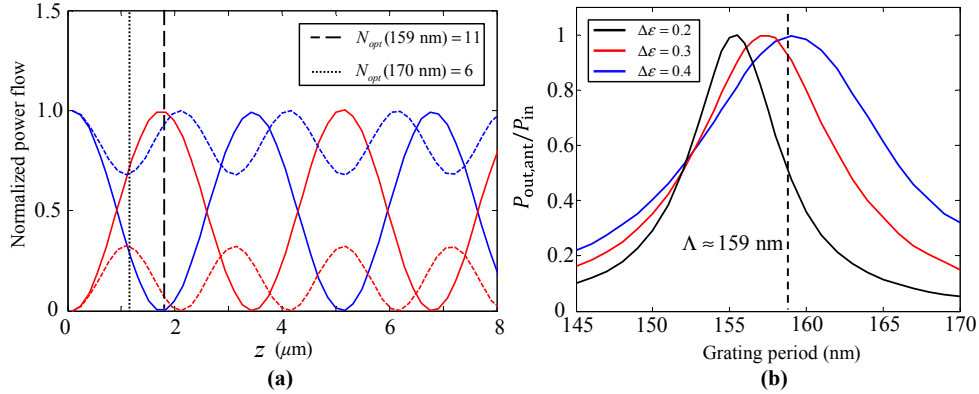


Fig. 3. (a) Normalized power flow for the symmetric (blue) and anti-symmetric (red) modes along the z -axis. The solid lines and dotted lines represent the cases for $\Lambda = 159$ nm and $\Lambda = 170$ nm, respectively. The grating strength is set to 0.4. (b) Normalized output power flow of the anti-symmetric mode as a function of grating period. The length of the grating is adjusted at N_{opt} number of periods for each grating period.

The response of the designed grating to pulses was examined by launching the pulse specified in the previous section. Figure 4(a) shows the normalized power transmission of the two modes for an incident symmetric mode pulse. It is observed that the symmetric mode at the central frequency is almost perfectly suppressed, but the conversion efficiency drops to zero as detuning increases to more than 3 nm. Hence, a considerable portion of the symmetric mode pulse remains unchanged, thus causing a complicated pulse profile, as shown in Figs. 4(c)-4(f). First, a portion of the symmetric mode pulse is converted to an anti-symmetric mode pulse and the two pulses then split due to a difference of group velocity. Some populations of the anti-symmetric modes are then transferred back into symmetric modes and, consequently, split symmetric and anti-symmetric mode pulses appear in the output.

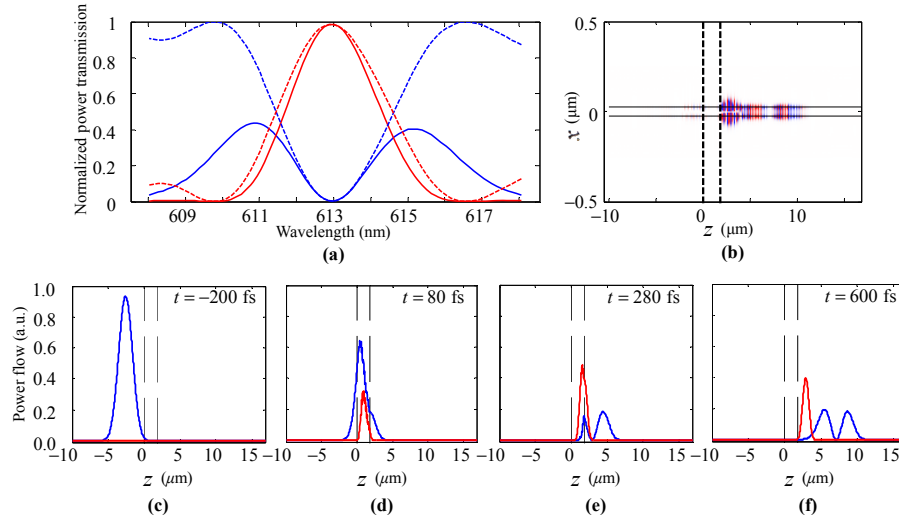


Fig. 4. (a) Normalized power transmission for a periodic grating. Dashed lines represent the normalized power transmittance spectrum and solid lines represent the output pulse spectra for Gaussian pulse input. (b) H_y field distribution after the pulse passed through the binary grating (Media 1). Snapshots of power flow profiles at (c) 200 fs before the peak of pulse enters the grating, and at (d) 80 fs, (e) 280 fs and (f) 600 fs after its entry. Red and blue lines mark anti-symmetric and symmetric modes, respectively.

A scheme using binary gratings might be sufficient, provided that it is enough to excite slow pulses at a desired position. However, a significant portion of input energy is wasted and the system bandwidth is severely limited. For optical information processing applications, it may be undesirable to pass residual symmetric mode pulses. Therefore, a broadband design that can successfully suppress symmetric mode output is essential. In the next section, we present a potentially simple solution to this issue.

4. Nearly perfect transition of the pulse by using chirped grating

In order to deal with the broadband design issue discussed above, we start with the origin of the problem that we already know, i.e. the fact that the grating is optimized only at the central frequency. Increasing the strength of perturbation may help because the spectra of the converted output become broader as shown in Fig. 3(b). However, such an approach is vulnerable to side effects including strong and complicated reflection spectra or unexpected coupling to modes other than the two waveguide modes under consideration. Instead, it is better to cascade binary gratings with different grating periods. Let us imagine a simple case in which we launch symmetric modes of frequencies ω_1 and ω_2 to two cascaded gratings that are tuned for each frequency. Their mode conversions will occur at different positions for two frequencies. While the mode transition occurs at the tuned grating, the modal population fluctuates weakly at the detuned grating. Extending the two cascade gratings to a nearly continuously chirped grating, high and uniform mode conversion efficiency over the spectral range of the input pulse would be expected. To examine possibility, we designed a chirped grating with a decreasing grating period as depicted in Fig. 5(a). The n^{th} grating period Λ_n is determined by the following recursive relation:

$$\frac{2\pi}{\Lambda_n} = \frac{2\pi}{\Lambda_{n-1}} + 0.006q_0, \quad (6)$$

where $2\pi/q_0 = 159$ nm corresponds to perfect phase matching for the central frequency. Because the grating periods that satisfy the phase matching condition for wavelengths of 608 nm and 618 nm are 177 nm and 141 nm, respectively, the local grating period range must include these values. In practice, a margin should be present at both ends to retain conversion efficiency over the entire spectral range of input pulse. Therefore, we chose the following values: $\Lambda_1 \approx 188$ nm and $\Lambda_{60} \approx 133$ nm.

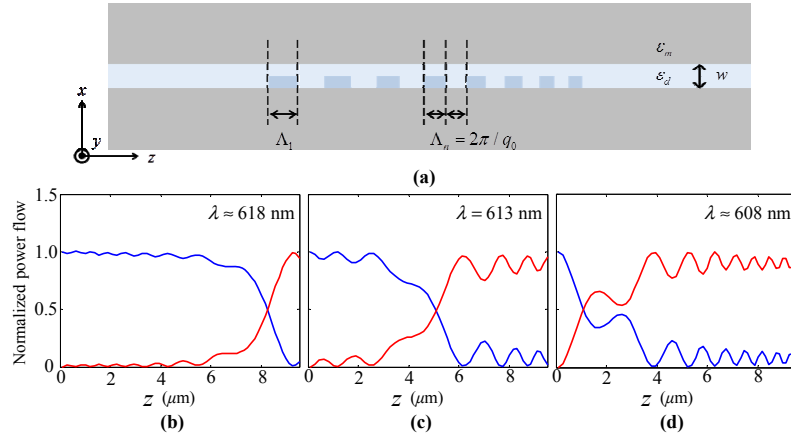


Fig. 5. (a) The up-chirped grating structure inside a MIM waveguide. Normalized power flow in the chirped grating at wavelengths of (b) 618 nm, (c) 613 nm and (d) 608 nm, respectively. Red and blue lines mark anti-symmetric mode and symmetric mode, respectively.

The mode transition behavior inside the chirped gratings are shown in Figs. 5(b)-5(d), confirming our predictions that a lower frequency mode requires a larger grating momentum for compensation, as deduced from Fig. 2. The results show that the transition point indeed shifts from the rear to the front as the wavelength decreases. We also observe that the fluctuation before and after the transition region is too small to significantly affect overall conversion efficiency.

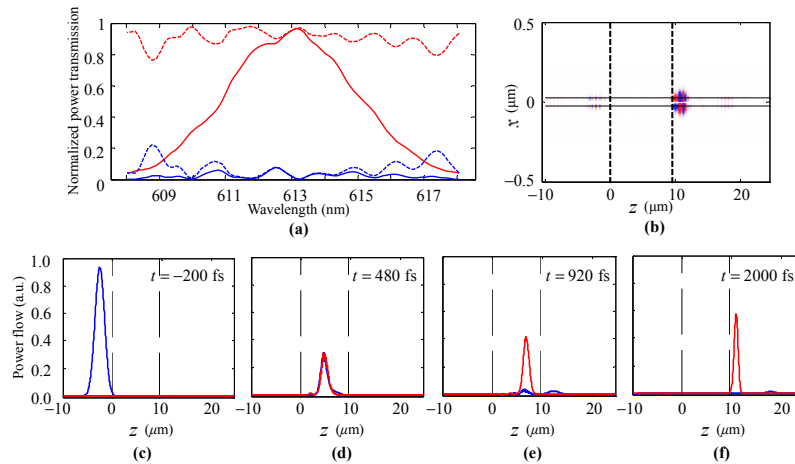


Fig. 6. (a) Normalized power transmission spectrum of chirped grating. Dashed lines represent normalized power transmittance spectra and solid lines represent the output pulse spectra for Gaussian pulse input. (b) H_y field distribution after the pulse passed through the chirped grating (Media 2). Snapshots of the power flow profile at (c) -200 fs, (d) 480 fs, (e) 920 fs and (f) 2000 fs. Red and blue lines mark the anti-symmetric mode and symmetric mode, respectively.

The resulting transmission spectrum of the designed chirped grating is shown in Fig. 6(a). The transmission spectrum of the symmetric mode is nearly perfectly suppressed while the transmission spectrum of the anti-symmetric mode is similar to the input pulse spectrum. Hence, a fast surface plasmon pulse has been nearly perfectly converted to a slow surface plasmon pulse. Figures 6(c)-6(f) show snapshots of the pulse conversion process, also confirming that the symmetric mode pulse is suppressed at the output.

Lastly, we conclude by discussing possible fabrication processes and measurement setups. For fabrication, a metal film should be deposited on a glass substrate and an in-coupling slit needs to be carved using a focused ion beam (FIB) technique. A silicon film should then be deposited and doped to form an asymmetric grating via the use of a mask with a grating pattern. Depositing a metal film once again and carving an out-coupling slit gives the desired device. For characterization of the fabricated device, the fact that the slow anti-symmetric mode entails more propagation loss than the symmetric mode can be exploited. First, multiple copies of the sample need to be fabricated, but the distance between the grating and the out-coupling slits should be different. From out-coupled light intensity data, it is possible to measure the decay characteristics after the grating and calculate the mode conversion efficiency. In order to confirm the broadband conversion characteristics, a tunable laser system can be used to measure its spectral properties.

7. Conclusion

A method for the efficient excitation of slow plasmonic pulses inside an MIM waveguide is proposed. A photonic interband transition induced by the grating was used as a mechanism to excite target modes at the desired position. FMM simulations confirmed that the mode transition behavior can be explained through coupled mode theory. Simple binary gratings optimized for a single frequency can excite slow pulses but residual fast mode pulses remain and the operating bandwidth is limited. On the other hand, that the use of a chirped grating, which can be considered as a cascade of small gratings with different grating periods, can significantly reduce residual pulses. This is because a chirped grating is effectively a cascade of gratings, each of which converts the symmetric mode to the anti-symmetric mode at different frequencies. The proposed scheme is preferable to tapering strategy for the design of active devices and it is expected to greatly simplify the temporal modulation profiles that are needed for active light trapping waveguide structures. Moreover, if a time dependent grating is employed, as discussed in [20–22], symmetric modes that are close to the light-line can be frequency up-converted to excite a slow surface plasmon pulse, resulting in a more dramatic reduction in group velocity. Hence, the extension of this work to dynamic structures may have significant implications for the development of surface plasmon buffers for photonic computing.

Acknowledgment

This work was supported by the National Research Foundation of Korea funded by Korean government (MSIP) through the Creative Research Initiatives Program (Active Plasmonics Application Systems).